PHYSICAL REVIEW B, VOLUME 63, 060407(R)

Nanometer-sized regions of charge ordering and charge melting in $La_{2/3}Ca_{1/3}MnO_3$ revealed by electron microdiffraction

J. M. Zuo
Department of Materials Science and Engineering and Materials Research Laboratory, University of Illinois at Urbana and Champaign, 1304 West Green Street, Urbana, Illinois 61801

J. Tao
Department of Physics and Astronomy, Arizona State University, Tempe, Arizona 85287-1504

(Received 2 October 2000; published 19 January 2001)

Electron microdiffraction study of phase transition in $La_{2/3}Ca_{1/3}MnO_3$ revealed temperature-dependent $(h+1/2,0,l)$ diffraction spots. Their intensity peaks at T_c. Quantitative electron diffraction intensity analysis shows that they come from nanometer-sized domains with modulated transverse atomic displacements in the orthorhombic a-c plane, which has two types of Mn ions and thus charge ordering. The average domain is ~3.6 nm in diameter and ~1.5 nm in height (along the b axis). The number of domains increases and then decreases, as the sample is cooled through T_c.

DOI: 10.1103/PhysRevB.63.060407 PACS number(s): 75.30.Vn, 71.38.−k, 61.14.Lj

Doped mixed-valent transition metal oxides exhibit complex temperature-dependent structural phases, which often have macroscopic crystal symmetry but with local structural fluctuations that resemble more closely the phases of liquid crystals.[1] An example is the phase separation found in high-T_c superconductors and related compounds.[2] Strong tendency of phase separation in manganites has also been predicted[3] and suggested by a number of experimental evidences.[4] However, so far, no clear picture has emerged about the structure and nature of phase separation. The reported length scale varies from subnanometer to micron.[4] Structural characterization is complicated by the microstructure of manganites, in the best case, as-grown single crystals are often twinned with submicron domains. Electron diffraction has the unique advantage for studying such structures. Single crystal diffraction pattern can be obtained from each domain, using a submicron electron probe. Using this approach, we observed the structural fluctuations in colossal magnetoresistive (CMR) $La_{2/3}Ca_{1/3}MnO_3$ by measuring electron diffraction intensity quantitatively. We find that the paramagnetic (PM) to ferromagnetic (FM) phase transition is accompanied by the formation and melting of random droplets of nanometer-sized domains. From the single-crystal electron diffraction data, we propose a structure model based on the structure of charge ordered $La_{1/2}Ca_{1/2}MnO_3$.[5] We show that there is a good agreement between the experimental diffraction intensity and the model, thus providing a strong evidence of charge ordering in these domains.

Upon cooling, doped $La_{1-x}Ca_xMnO_3$ (with $0.2<x<0.45$) undergoes a PM to FM transition at T_c, which coincides with a insulator-metal transition.[6] This, and related compounds, has attracted great attention recently because of CMR and the interesting physics. Structurally, $La_{1-x}Ca_xMnO_3$ has an average distorted-perovskite structure, with simple perovskite structure by $a \approx c \approx \sqrt{2}a_p$ and $b \approx 2a_p$. Accumulated experimental evidences suggest both structural and magnetic inhomogeneities.[3] Structural probe[7–9] revealed a gradual transition from multiple Mn-O bond lengths at high temperature characteristic of Jahn-Teller distortions, to a low-temperature single Mn-O bond length.

We use electron diffraction (ED) to study structural fluctuations near the phase transition because electrons interact strongly with crystals, and ED patterns can be obtained from a very small volume, and thus very sensitive to local structural fluctuations. The ED experiment was carried out using an energy filtering LEO-912Ω electron microscope (120 kV). Single crystal ED patterns were recorded from a thin area of 300 nm in diameter using parallel illumination.[10] The specimen is a polycrystalline $La_{2/3}Ca_{1/3}MnO_3$, thinned for electron transparency. The sample was synthesized by mixing stoichiometric proportions of La_2O_3, $CaCO_3$ and MnO_2 (puratronic grade, AESAR) using the standard solid state reaction method. Powder x-ray diffraction and energy-dispersed x-ray analysis in a electron microscope confirm a single-phase and chemically homogeneous structure within the experimental error. The sample was initially cooled with liquid nitrogen and measured by heating the specimen using the Gatan liquid nitrogen holder. The sample sits in a 1 T magnetic field from the electron objective lens. An energy selection slit of 10 eV was placed around the zero-loss peak to remove the inelastic background, which usually dominates the weak structural diffuse scattering in electron diffraction.[10] All diffraction patterns were recorded from the same area in the zone axis orientations using a beam divergence of 0.13 mrad, exposure time of 9 s and the camera length of 450 mm. Fuji 25 μm imaging plates were used for quantitative electron intensity recording. To compare diffraction intensity at different temperatures, we monitored the electron beam intensity and any change in diffraction conditions using the weak $\pm(104)$ and $\pm(104)$ reflections. The overall fluctuations were less than 6%.

Figure 1 shows the recorded electron diffraction patterns in the [010] zone axis orientation at four different temperatures.[11] The most remarkable feature in the diffraction pattern is the nearly commensurate satellite peaks with half indices of $(h+1/2,0,l)$; these are superlattice reflections from a superstructure with the period twice the original a axis. Previously, they were found in $(LaPrCa)MnO_3$ with Ca concentration of $x=3/8$.[12] The SR intensity changes with temperature, and they are most visible near T_c. The SR sits

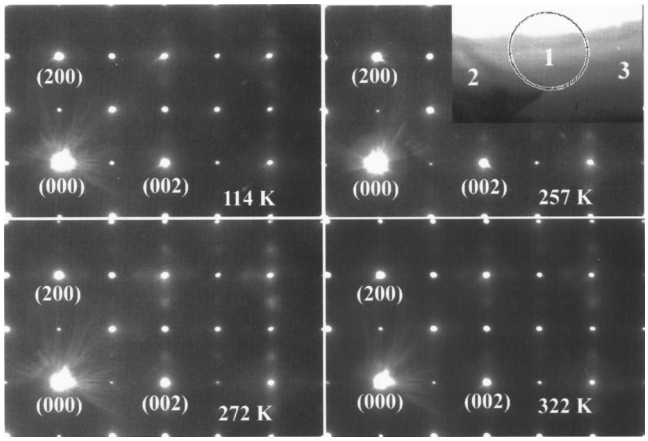

FIG. 1. Evidence of the temperature-dependent $x=1/2$ type charge ordering in $La_{2/3}Ca_{1/3}MnO_3$. Four diffraction patterns in the [010] zone axis orientation at (a) 114 K, (b) 257 K, (c) 272 K, and (d) 322 K are shown, displayed on an absolute intensity scale in units of counts (1 count corresponding to about 1.2 beam electrons). The diffraction patterns were taken from the circled region of the sample (shown in the up-right inset). The circle diameter is 0.3 μm. Three twin domains are visible in the image. The illuminated area covers a very small part of neighboring twins (2 and 3), giving the faint diffraction spots at the $(h+1/2,0,l+1/2)$ positions.

on a broad anisotropic diffuse background, especially near strong fundamental reflections. The diffuse scattering has the characteristics of Huang scattering. Figure 2(a) shows the intensity profile from (0, 0, 4) to (2, 0, 4) in Fig. 1. Both the SR intensity and the background change with temperature. The overall temperature dependence was measured using (3/2, 0, 4) SR. The results are shown in Figs. 2(b) and (c). The superlattice peak and background were separated by fitting the intensity distribution around (3/2, 0, 4) with a Gaussian function plus a linear background. From Fig. 2, we estimate $T_c \sim 270$ K. Figure 2 also shows that the increase in the satellite peak intensity is associated with an increase in the background, indicating that there is strain associated with the formation of the superstructures.

The SR is mostly observed in the [010] zone axis. Inspection of the [001] and [100] zone axes revealed anisotropic diffuse scattering, but no SR. The diffuse scattering observed here differs from that of Sr-substituted manganites.[13] In that case, incommensurate satellite peaks were observed at much smaller q, and the diffuse scattering disappeared almost entirely below T_c. The diffuse scattering observed in layered Sr doped manganites is mostly quasielastic.[13] The energy resolution of this experiment is not sufficient to make this distinction.

There are two coherence lengths in the diffraction pattern. The lattice reflection has a Gaussian half width (GHW) of 0.0053 Å^{-1}, of which 80% comes from the electron beam divergence, the rest from the detector and small-angle diffuse scattering due to atomic vibrations and strain. The GHW of SR, subtracted off the GHW of the lattice reflection, corresponds to structural domains of about 36 ± 2 Å in diameter. No appreciable change was observed in the half width of SR

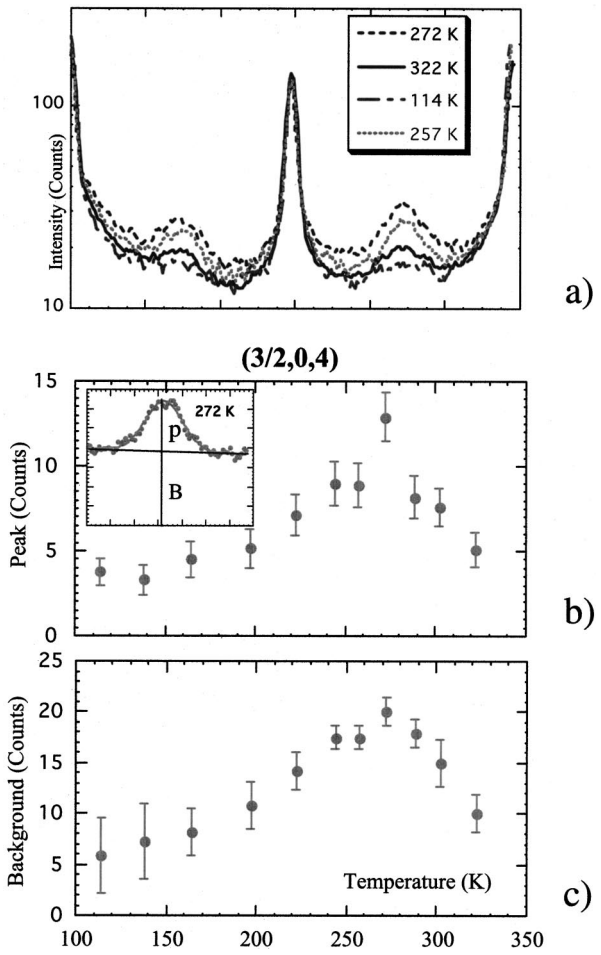

FIG. 2. Temperature dependence of diffraction intensities. (a) Intensity profiles of Fig. 1 from (004) to (204), averaged over a width of 0.008 Å^{-1}. The profiles clearly show two coherence lengths. The width of superlattice reflections corresponds a real space size ~36 Å; (b) the superlattice peak and (c) background intensity at (3/2,0,4) position as a function of temperature. The peak and background were obtained by fitting the intensity profile of (a) around (3/2,0,4) using the combination of a Gaussian function and the linear background [see the inset in (b)].

as a function of temperature. All these indicate that superlattice reflections come from nanodomains, of nearly constant sizes.

The diffraction pattern of Fig. 1 has the characteristics that come with an atomic displacement wave. Superlattice reflections are nearly absent in the $(h+1/2,0,0)$ row, and strong superlattice peaks are associated with strong fundamental reflections in the $l=2n$ rows. Both suggest that superlattice peaks originate predominately from small atomic displacements. In such case, kinematical diffuse scattering is given by:[14]

$$F_k(\mathbf{G}+\mathbf{q}) \propto (\mathbf{G}+\mathbf{q}) \cdot \sum_i \mathbf{\Delta}_i f_i \exp[-W_i(\mathbf{G}+\mathbf{q})] \times \exp(2\pi i \mathbf{G}\cdot\mathbf{r}_i). \quad (1)$$

The observed extinction of $(h+1/2,0,0)$ reflections and $(h+1/2,k,0)$ reflections in the [001] zone axis can be explained

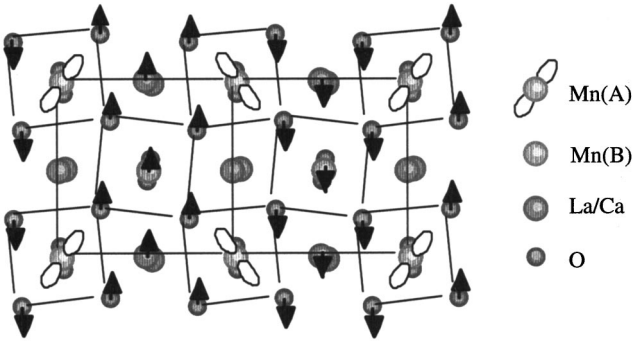

FIG. 3. Atomic structure model of lattice distortions proposed for the superstructure. In this model, atoms shift by $\pm\Delta$ and 0 depending on their position (as indicated by the arrow). The displacement pattern resembles a transverse wave with $k=(1/2,0,0)$.

by the $(\mathbf{G}+\mathbf{q})\cdot\mathbf{\Delta}$ term with $\mathbf{\Delta}$ parallel to the c axis. Based on this, we propose a model (Fig. 3) for the superstructure inside the nanodomains. In this model, atoms are displaced along the c axis with a pattern that closely resembles a transverse wave of $q=(100)/2$. Transverse atomic displacement wave was previously obtained in the charge-ordered phases of $La_{1/2}Ca_{1/2}MnO_3$ (Ref. 5) and $La_{2/3}Ca_{1/3}MnO_3$.[18]

The displacements shown in Fig. 3 result two types of Mn ions, Mn(A) and Mn(B). For the Mn(A), four oxygens with two each at the left and right move in opposite directions. These gives two short and two long Mn-O bonds in the $a-c$ plane, and they differ by $\sim\Delta/\sqrt{2}$. The Mn(B) ion is unchanged and has nearly equal bond lengths. Atomic pair distribution from x-ray results[9] indicate three bond lengths ($\sim$1.85–1.9 Å, $\sim$1.97 Å, and $\sim$2.1–2.15 Å) at 300 K and a single bond length at 20 K for $x=0.33$. Assuming that the different bond-lengths are due to charge ordering, we expect the shortest bond of $\sim$1.9 Å for the Mn^{4+}-O^{2-} bond. This can be accounted for by introducing a contraction (δ) for the Mn^{4+}-O^2 bond in the $a-c$ plane and a consequent dilation for the Mn^{3+}-O^{2-} bond in the same plane. To fit the x-ray data, we need $\Delta\sim0.14$ Å and $\delta\sim0.06$ Å. For comparison, the mean thermal displacement of oxygen in this material is about 0.09 Å.

To see whether the model proposed above fits the experimental data, we carried out a full dynamical calculation of electron scattering from randomly distributed structural domains, assuming incoherent electron scattering from each domain. Dynamic calculations are necessary because of strong electron scattering. Theoretically, whether the nanostructures are static or time dependent, they can be treated similarly by averaging over space or time or both. We use the general dynamic theory of electron diffuse scattering derived by Gjonnes,[15] taking account of electron diffraction before and after the diffuse scattering:

$$dI(q+h)=dz\sum_{g}\sum_{g'}\sum_{f}\sum_{f'}S_{hg}(2)S^{*}_{hg'}(2)f_1 \times(q+g-f)f^{*}_{1}(q+g'-f')S_{of}(1)S^{*}_{of'}(1). \quad (2)$$

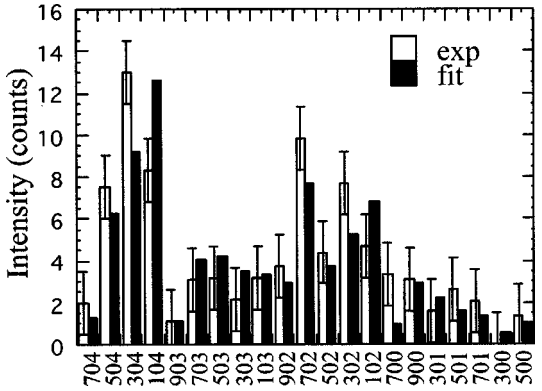

FIG. 4. A comparison between the experimental and theoretical dynamic diffraction intensities of superlattice reflections. The reflection index (x axis) is based on the supercell. Theoretical intensities were calculated using the structure model proposed in Fig. 3, and the domain thickness of 15 Å.

Here f_1 is the electron scattering matrix of the superstructure and $S_{of}(1)$ and $S_{gb}(2)$ are the scattering matrices from the averaged structure before and after the superstructure, respectively. All are calculated using the Bloch wave theory of electron diffraction.[16] The calculation was done by integrating Eq. (2) over the sample thickness, which we estimate to be 840 Å from the intensities of fundamental reflections. The SR structure factors were calculated using $\Delta=0.14$ Å (they are not affected by the contraction δ). The thickness of nano-domains, t, was treated as a parameter. The calculation was compared with 21 independent superlattice reflections in the [010] zone axis. The best fit between theory and experiment was obtained with $t\sim15$ Å, which has a $\chi^2\sim1.4$. The comparison between our model and experiment is shown in Fig. 4. The agreement is good, considering that the model only contains a single structural parameter. From the intensity of SR, we estimate the volume percentage of nanodomains to be a few percent at 272 K with $\Delta=0.14$ Å. This estimate is inversely proportional to Δ^2.

The nature of superlattice reflections cannot be explained by simple chemical inhomogeneity, however, it is possible that fluctuations in chemical composition could act as the pinning centers for charge ordering. Experimentally, it is also not clear whether the $x=1/2$ type charge ordering is associated with an excess concentration of 1/6 holes per formula inside the nano-domain. Charge separation, in general, is not favored energetically. The amount of Coulomb energy required to separate charges increases rapidly with the size (In the textbook case of a spherical charge cloud of radius r, the assembly energy is proportional to r^5.) Charge separation can only exist if there is a sufficient amount of energy gained by charge ordering, which would be proportional to the volume (r^3). In that case, the size of charge separated domains would be dictated by the balance between the Coulomb interaction and charge ordering.

The experimental picture emerged from our electron diffraction study can be summarized in following. Above T_c, there is an average increase in the number of extended ordered structural domains, as the sample is cooled toward T_c. Below T_c, the average number of domains slowly decreases.

The shape of domain resembles a droplet, with the diameter ~36 Å and height ~15 Å (along the *b* axis). They are randomly distributed. Recent neutron data shows that they are also static with a lifetime larger than 1 ps (Ref. 17) ($t > 3\,\mu$s from the NMR data[19]). Compared to the average structure, the domain has modulated transverse atomic displacements in the *a*-*c* plane, similar to these found in the structure of charge ordered $La_{1/2}Ca_{1/2}MnO_3$. The rise and fall of superlattice reflections coincide with the similar change in resistivity, indicating that they are strongly related. The experimental findings here raise interesting questions about the underlying physical origin of these domains, their effect on the transport properties, and the implied charge separation associated with charge ordering.

This work was supported by the U.S. Department of Energy (Division of Materials Sciences, Office of Basic Energy Sciences) under Grant No. DEFG02-91ER45439 (J.M.Z.). The experiment was done at the Center for HREM, ASU and supported by NSF DMR9973894. The authors thank Professor J. Spence and M. Salamon for comments.

[1] S. A. Kivelson, E. Fradkin, and V. J. Emery, Nature (London) **399**, 550 (1998).

[2] *Phase Separation in Cuprate Superconductors*, edited by E. Sigmund and K. A. Müller (Springer, Berlin, 1994).

[3] For a review, see A. Moreo, S. Yunoki, and E. Dagotto, Science **283**, 2034 (1999).

[4] J. M. De Teresa *et al.*, Nature (London) **386**, 256 (1997); M. Fath *et al.*, Science **285**, 1540 (1999); M. Hennion *et al.*, Phys. Rev. Lett. **81**, 1957 (1998); S. H. Chun, M. B. Salamon, Y. Tomioka, and Y. Tokura, Phys. Rev. B **61**, R9225 (2000); M. Jaime *et al.*, *ibid.* **60**, 1028 (1999) and Ref. 12.

[5] P. G. Radaelli, D. E. Cox, M. Marezio, and S.-W. Cheong, Phys. Rev. B **55**, 3015 (1997).

[6] P. Schiffer, A. P. Ramirez, W. Bao, and S.-W. Cheong, Phys. Rev. Lett. **75**, 3336 (1995).

[7] S. J. Hibble *et al.*, J. Phys.: Condens. Matter **11**, 921 (1999).

[8] C. H. Booth *et al.*, Phys. Rev. B **57**, 10 440 (1998).

[9] S. J. L. Billinge *et al.*, Phys. Rev. B **62**, 1203 (2000).

[10] G. Benner, J. Bihr, and E. Weimer (unpublished); J. M. Zuo, J. Pacaud, R. Hoier, and J. C. H. Spence, Micron **31**, 527 (2000).

[11] Read close to the sample; temperature at the illuminated area could be slightly high due to electron beam heating.

[12] M. Uehara, S. Mori, C. H. Chen, and S.-W. Cheong, Nature (London) **399**, 560 (1999).

[13] L. Vasiliu-Doloc *et al.*, Phys. Rev. Lett. **83**, 4393 (1999).

[14] M. A. Krivoglaz, *X-ray and Neutron Diffraction in Non-Ideal Crystals* (Springer, Berlin, 1996).

[15] J. Gjonnes, Acta Crystallogr. **20**, 240 (1966).

[16] J. C. H. Spence and J. M. Zuo, *Electron Microdiffraction* (Plenum, New York, 1992).

[17] After finishing this paper, we became aware of two neutron measurements on single crystal $La_{1-x}Ca_xMnO_3$ [C. P. Adams *et al.*, Bull. Am. Phys. Soc. **45**, 528 (2000); P. Dai *et al.*, Phys. Rev. Lett. **85**, 2553 (2000)]. The neutron measurements revealed the same half-index charge ordering diffraction spots observed here and similar temperature dependence. The neutron measurement shows that the superlattice reflections are elastic with time scale $t > 1$ ps. The difference between the neutron measurement and the present electron measurement is that the neutron data is averaged over several twin orientations and over a large volume. The average correlation length measured by neutrons ranges from 10 to 28 Å. The present study shows a short correlation length along the *b* axis (~15 Å) and a longer one in the *a*-*c* plane (~36 Å).

[18] R. Wang, J. Gui, Y. Zhu, and A. R. Moodenbaugh, Phys. Rev. B **61**, 11 946 (2000).

[19] G. Papavassiliou *et al.*, Phys. Rev. Lett. **84**, 761 (2000).